IEEE Access
Multidisciplinary | Rapid Review | Open Access Journal

Received March 30, 2020, accepted April 4, 2020, date of publication April 13, 2020, date of current version April 30, 2020.

Digital Object Identifier 10.1109/ACCESS.2020.2987556

Sustainable, Portable, and Efficient Electricity Delivery (SPEED): Design, Control, and Testing

SANKA LIYANAGE[1], (Member, IEEE), YEQIN WANG[2], (Member, IEEE), YITING DONG[1], (Graduate Student Member, IEEE), AND BEIBEI REN[1], (Senior Member, IEEE)

[1]Department of Mechanical Engineering, Texas Tech University, Lubbock, TX 79409, USA
[2]National Wind Institute, Texas Tech University, Lubbock, TX 79409, USA

Corresponding author: Yeqin Wang (yeqin.wang.1987@ieee.org)

ABSTRACT During emergencies or natural disasters, or at remote areas, the main electrical grid might be damaged or not accessible, therefore, a sustainable electricity generation is critical for human survivals or other electricity needs. This paper presents a sustainable, portable, and efficient electricity delivery (SPEED) system for community emergency, disaster relief, and power supply at remote areas. A demonstrated system with utility-level AC power output is built up with a 180 W photovoltaics (PV) array which consists of six serial-connected solar panels, a 1.8 kWh battery pack, a SYNDEM power converter, and a data monitoring subsystem. The autonomous operation of the system is achieved by advanced control technologies for power electronic converters in both islanded mode and grid-connected mode, while providing the overcharging and overdischarging protections of the battery pack. Field testing is conducted to validate the effectiveness of the proposed SPEED system under different scenarios.

INDEX TERMS Sustainable portable electricity, solar energy, emergency/disaster relief, power electronics control, battery protections.

NOMENCLATURE

V_{PV}	PV voltage.
I_{PV}	PV output current.
P_{pv}	PV output power.
V_{pv}^*	PV voltage reference.
V_b	Battery voltage.
V_{b01}, V_{b02}, V_{b03}	Battery voltage protection trigger points.
D_V, D_P, D_E	Droop coefficients for battery protection.
u	Duty cycle for DC/DC converter.
P_g, Q_g	Real and reactive power outputs of DC/AC converter.
P_g^*, Q_g^*	Real and reactive power references
E	RMS output voltage of DC/AC converter.
δ	Power angle.
U_g	RMS voltage of the main grid or loads.
Z_0	Output impedance amplitude of DC/AC converter.
θ	Output impedance angle of DC/AC converter.
ω	Frequency of the DC/AC converter.
ω^*	Rated frequency of AC grid.
E^*	Rated RMS voltage of AC grid.
m, n	Droop coefficients for real and reactive power.
i_g	Instantaneous current of DC/AC converter.
u_g	Instantaneous voltage of the main grid or loads.
$\triangle_p$, $\triangle_q$	Lumped uncertain terms.
η	Approximated system efficiency.

The associate editor coordinating the review of this manuscript and approving it for publication was Yang Li.

I. INTRODUCTION

Incorporation of sustainable and portable electricity generation to support critical electricity demands is important for improving community resiliency and energy independence. Recent studies show that the main electrical grid disconnection is the major disruption to the current status quo of the human life [1], [2]. In the United States, severe weather such as thunderstorm, hurricane and blizzard is the leading cause of power outages. Reports show that roughly 679 widespread power outages between 2003 and 2012 are caused by weather events, which cost annual average of $18 billion to $33 billion US dollars [3]. For example, the superstorm Sandy

knocked out power for 8.5 million customers, and hurricane Irene affected more than 6.5 million people with power loss [3]. Recently, hurricane Irma cut power to nearly two-thirds of Florida's electricity customers [4], and more than quarter-million people were affected by Texas power outage caused by Hurricane Harvey [5]. Therefore, tremendous critical needs are being reported in the literature for power preparation for the community's survivals during extreme emergencies [6]–[8]. In remote monitoring applications, such as oil field monitoring systems, pipeline monitoring systems, etc., communications and critical electronic systems also require continuous electricity supplies [9], [10]. To address above power demands, the portable and sustainable electricity delivery system is one of the promising solutions. During an aftermath of a natural disaster, the electric grid might be not available for a long period, and the conventional portable electricity delivery systems, e.g., fuel-based generators, may experience serious challenges with insufficient or unavailable fuels. Furthermore, using gasoline or diesel generators to generate the electricity may not be the most economically feasible and practical solution due to the following drawbacks of conventional generators: insufficiency under low load operation, high maintenance cost, sound pollution, high greenhouse gas pollution and scarcity of fossil fuel supplies [11], [12]. Alternatively, a modularized portable renewable energy-based solution can be used to achieve aforementioned power demands and to cope with the drawbacks of conventional generators [13].

This paper presents a sustainable, portable, and efficient electricity delivery (SPEED) system for community emergency/disaster relief and power supply at remote areas, where a photovoltaics (PV) source and a battery pack are integrated by power electronic converters with standard utility-level AC output [14]. The main functions of the SPEED system include islanded mode operation with the grid-forming capability for outdoor activities; grid-connected mode operation at normal daily scenarios, where the energy generated by the PV source can be sent to the main grid; the maximum power acquisition from the PV source for improving the energy efficiency; and battery protections to avoid both overcharging and overdischarging. The power electronics control plays the key role to facilitate these functions. It is worth noting that several other factors also should be considered for the PV-based portable electricity delivery system, such as the PV size, battery capacity, strength of the mounting platform, etc., and more information can be found in [13]. This paper focuses on the power electronics control for the flexible operations of the SPEED system.

The control challenges associated with the autonomous operation of the SPEED system are listed as follows. Firstly, in the traditional grid-integration of the PV source or the battery pack, the power converters are usually operated as current sources [15], where a dedicated phase-locked loop (PLL) is required for grid synchronization [16]; while in islanded mode [17], [18], they should be operated as voltage sources to provide both voltage and frequency regulation, where the PLL is not required for the continuous operation. These two incompatible sources for different operation modes would complicate the control system design for the SPEED system. Secondly, the SPEED system needs to be scalable and capable of working at parallel mode, and it is expected that multiple different-scale SPEED systems can work together to conduct emergency/disaster relief. The grid-forming converter should be designed for the SPEED system with the black-start capability at both stand-alone operation or parallel operation. When multiple grid-forming converters work together, one challenge is how to make sure all interconnected units could work together and maintain system stability, i.e., voltage and frequency regulation; and the other challenge is how to achieve power sharing among these units. If the power is not well shared, the circulation currents may occur among interconnected units, which may trigger the protection of the power electronic converters, or cause the damage. For example, though both grid-connected mode and islanded mode operations of the PV-battery system are studied in [16], the droop functions are not considered, therefore, this kind of system is lack of scalability. Thirdly, the maximum power acquisition of the PV source is usually achieved through maximum power point tracking (MPPT) algorithms [16], [19], e.g., the P&O MPPT algorithms [20], [21]. If the PV power is larger than the load consumption in islanded mode, the extra power will be stored in the battery pack, and the battery pack might be overcharged during the long-term operation. Though some PV power-limited control algorithms are proposed in [16], [20]–[22] to avoid the battery overcharging, the direct power regulation or direct current regulation of the PV source is considered, which might cause the power oscillation or current oscillation [20], specially, under the varying condition of the solar irradiation. A constant voltage control strategy of the battery voltage is provided in [23] to limit the PV power, however, the battery voltage cannot be well regulated if the PV is shaded. Fourthly, the battery pack might be overdischarged if the whole system is not well regulated within different operation scenarios. All these scenarios will degrade the lifespan of the battery pack, or even cause the fire hazard. Finally, in most of PV-storage or PV-battery systems, the central power management systems or energy management systems are usually required for the operations of different modes, and the decisions of mode changes [16], [20], [21], [24].

In this paper, the advanced power electronics control technologies are developed to achieve the autonomous operation of the SPEED system at both islanded mode and grid-connected mode. For islanded mode operation of the SPEED system, particularly for emergency/disaster relief, a voltage source-based robust droop control strategy, named the uncertainty and disturbance estimator (UDE)-based robust droop control technology [18], is adopted to operate the power electronic converter as a grid-forming converter. It is an improved version of the conventional droop controller [25] by introducing the load-voltage feedback and the UDE-based robust control algorithm. It can achieve autonomous black-start,

accurate power sharing, good voltage/frequency regulation, and good performance to handle the uncertainties and disturbances from loads or output impedance. It also inherits the advantages of the conventional droop control, such as, no communication requirement, autonomous power balance between source side and load side, and "plug and play" feature, which enables the potential parallel operation of multiple different-scale SPEED systems. For grid-connected mode operation of the SPEED system, the voltage source-based robust power flow control [26] is introduced to achieve a grid-friendly manner and to reject various disturbances, such as the fluctuations of the battery voltage, variations of output impedance or line impedance, and variations of the grid voltage. With the voltage sources adopted for both islanded mode and grid-connected mode, the robust droop control and robust power flow control can be integrated into a unified control framework, which simplifies the control system design.

In addition, an extremum seeking (ES)-based MPPT algorithm [27], [28] is adopted for maximum power acquisition of the PV source. The ES algorithm, one of the P&O MPPT methods, can always capture maximum power of the PV source. In order to avoid the possible battery pack overcharging caused by the ES-based MPPT, a ''PV voltage droop control'' algorithm based on the battery voltage is proposed to avoid this issue. When the battery voltage is higher than a voltage-protection trigger point, the PV voltage reference will be adjusted accordingly to decrease the power output of the PV source. The idea of this design is motivated by the conventional droop control [25], [29] for AC voltage and frequency regulations. Therefore, the name of ''droop control'' is also adopted in this design. Besides, in grid-connected mode operation, a ''real power set point droop control'' algorithm based on the battery voltage is developed to keep the power balance of the battery pack without overcharging or overdischarging, where the real-power reference will be adjusted according to the battery voltage. Furthermore, in islanded mode operation, an ''AC voltage set point droop control'' algorithm based on the battery voltage is proposed to further prevent the overdischarging of the battery pack, where the AC voltage set point will be reduced when the battery voltage is lower than a voltage-protection trigger point. Therefore, the proposed design can naturally avoid both overcharging and overdischarging of the battery pack without any additional protection actions at different operation scenarios.

For system demonstration, a SPEED prototype system with a 180 W PV array which consists of six serial-connected solar panels, a 1.8 kWh battery pack, a SYNDEM power converter [30], and a data monitoring subsystem is built up. The SYNDEM power converter is utilized as the power electronic interface to integrate both the PV array and the battery pack with standard utility-level AC output, and all the proposed advanced control technologies are embedded into the SYNDEM power converter. Moreover, a Raspberry Pi-based real-time data monitoring subsystem and a dynamic web-server are developed for local and remote data monitoring. Furthermore, the system is built on a mobile platform to enhance the portability. The field test of this SPEED platform was conducted on Texas Tech University (TTU) campus with both islanded mode and grid-connected mode operations.

The main contributions of this paper are highlighted below:

- A SPEED system is developed for applications associated with community emergency, disaster relief, and power supply at remote areas with sustainable power solutions. Advanced power electronic control technologies are developed and implemented to achieve the autonomous operation of the SPEED system at both islanded mode and grid-connected mode. A SPEED prototype system is built and tested with both islanded mode and grid-connected mode operations on TTU campus.
- The voltage source-based control techniques are adopted for the control of the SPEED system at both islanded mode and grid-connected mode without the requirement of PLL. In particular, a unified control framework is provided to integrate the robust droop control for islanded mode operation and the robust power flow control for grid-connected mode operation. This enables the grid-forming capability and the scalability of the SPEED system, and parallel operation of multiple different-scale SPEED units.
- The proposed PV voltage droop control algorithm is designed through the setting of the PV voltage reference based on the battery voltage. With the introduction of the hysteresis band for the battery voltage trigger point, the power oscillation can be naturally avoided during the limited power operation of PV source, even under the varying condition of the solar irradiation or shading. With the combination of the real power set point droop control, and the AC voltage set point droop control, both overcharging and overdischarging of the battery pack at different operation scenarios can be naturally avoided.
- In the proposed design, the DC-DC converter and the DC-AC converter can be operated independently. The ES-based MPPT and PV voltage droop control can be automatically switched based on the battery voltage. The unified control framework can automatically determine the operation modes, and the battery pack charging or discharging. It does not require the extra power management system or energy management system to regulate power flow for PV source, battery pack, and AC loads/grid under different operation modes, which greatly simplifies the control design. Indeed, all the proposed control design and communication design are achieved in a widely-used Texas Instruments (TI) TMS320F28335 microcontroller unit (MCU) with a sampling time of 150 μs for power electronics control and a sampling time of 0.1 s for RS485 communication, which enhances the feasibility of the proposed SPEED system.

The preliminary results of this work were published at 2019 IEEE Green Technologies Conference [31]. Compared with

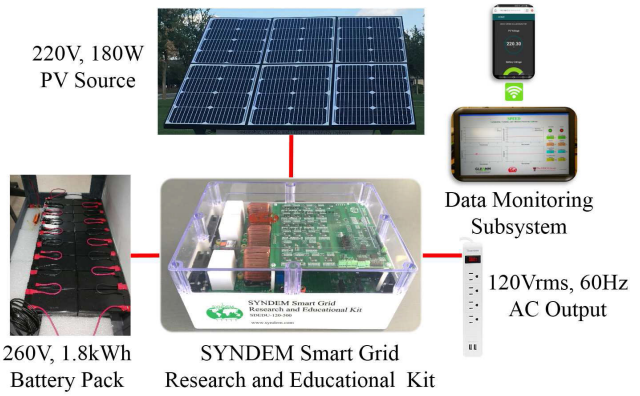

FIGURE 1. The system design of the SPEED system.

our preliminary results in [31], this paper provides a thorough design and test of the SPEED system. The detailed control structure and control algorithms are proposed for the autonomous operation of the SPEED system at both islanded mode and grid-connected mode. Three aspects of battery protection algorithms are further illustrated. Moreover, extensive experimental results with the operations of the proposed system under different modes and different battery protections are provided to demonstrated the effectiveness of the proposed design.

The remainder of the paper is as follows. Section II describes the SPEED system design. The advanced power electronics control and the data monitoring subsystem design are presented in Section III. Results of field experiments are shown in Section IV. The final Section V concludes the whole paper.

II. SYSTEM DESCRIPTION

Fig. 1 shows a SPEED prototype system, which consists of a 180 W PV source, a 1.8 kWh battery pack, a SYNDEM power converter, and a data monitoring subsystem. The solar panels absorb solar energy and convert it into DC power. The battery pack is used for energy storage. The SYNDEM power converter provides the power electronic interface for both the PV source and the battery pack with standard utility-level AC output. The data monitoring subsystem is designed for monitoring and recording real-time data of the SPEED system.

The 180 W PV source includes six serial-connected ALEKO SP30W24V-AP solar panels (30 W each). The fitting curves based on a popular five-parameter model [32], [33] and the specifications of the ALEKO SP30W24V-AP solar panel for the PV source are shown in Fig. 2. The MPPT algorithm is needed to achieve the maximum power acquisition of the PV source, because both output current and output power of the PV source are variable to different load conditions and solar irradiations. From Fig. 2, it is clear that, the optimal operated condition of this PV source is at the point with 220 V and 0.82 A, when the solar irradiation is 1000 W/m^2. The reason for the high voltage, low current PV source design is to increase the system efficiency with less power losses.

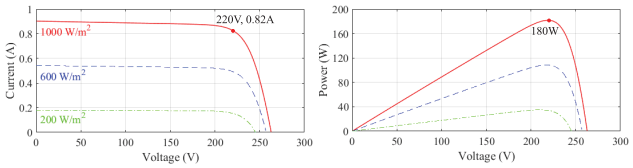

(a) Current-voltage curve (b) Power-voltage curve

FIGURE 2. The approximated model for the PV source at different solar irradiation conditions and $T = 25°C$.

In this design, 20 rechargeable lead-acid batteries (12 V @ 8 Ah each) are integrated as a battery pack, and the maximal available energy storage capacity is about 1.8 kWh. The major function of the battery pack is to balance the fluctuations of both PV power and load consumption. Though the PV source can operate at the optimal point with the MPPT function, the optimal point still varies at different solar irradiations, such as daily changes or shading effects. In another aspect, the load consumption usually is different from the instantaneous PV power. Therefore, the battery pack should store the energy when the PV source is sufficient, and release the energy when more power is required by the loads.

In this work, the SYNDEM Smart Grid Research and Educational Kit or the SYNDEM power converter, a MathWorks third-party product [30], is performed as the power converter to integrate the PV source, the battery pack with the standard utility-level AC outputs. It is a multifunctional power electronic converter to facilitate research and education in grid integration of various renewable energy sources, such as solar power, wind power, and energy storage systems, and flexible loads. This kit can be reconfigured to obtain 10+ different power electronic converters, versatile for different applications. It also includes both RS485 and CAN communication interfaces to send both system data and control data out. In the SPEED system, the SYNDEM power converter is configured as a DC/DC boost converter and a single-phase DC/AC converter, as shown in Fig. 3. In this design, the battery pack is directly linked to the DC-bus to increase system efficiency. While the DC/DC boost converter converts DC power of the PV source into the battery pack, and the single-phase DC/AC converter feeds the DC power from both the PV source and the battery pack into AC load or AC grid. It is worth noting that a standard power electronics module with three legs is enough to cover the topology of the SPEED system, and the SYNDEM power converter can be used to connect the PV source and the battery pack with utility-level AC output for AC loads or AC main grid. There might exist some drawbacks to connect the battery pack to the DC-bus directly. For example, more battery units are required to integrate the battery pack, if 12V lead-acid batteries are considered; and a large DC-bus capacitor is required to filter the harmonics from both the DC-DC converter side and the DC-AC converter side.

The SPEED platform also consists of a real-time data monitoring subsystem, which runs on a Raspberry-Pi single board computer. The SYNDEM power converter communicates

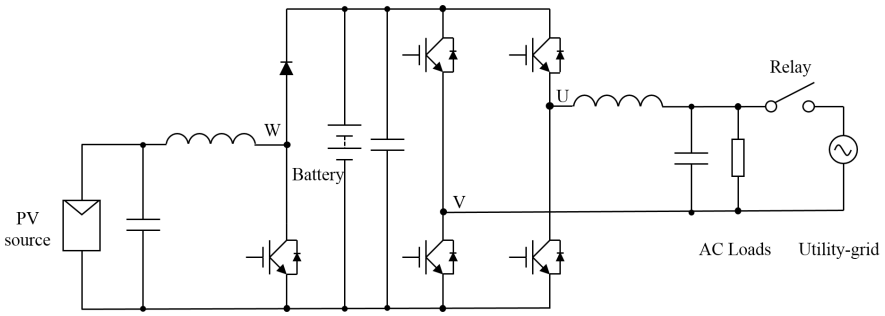

FIGURE 3. The topology of the SPEED system with a DC/DC converter and a DC-AC converter.

with the data monitoring subsystem via a RS485 channel. A graphical user interface (GUI), which is displayed on a 17-inch UHD, is used to display the real-time data trace. To enable remote monitoring capabilities, a dynamic web server running on a Raspberry-Pi single board computer is provided. The Raspberry-Pi also operates as a Wi-Fi access point for users to monitor real-time data on mobile devices via the web server.

This SPEED system can be operated at both islanded mode and grid-connected mode. If the SPEED system is deployed for outdoor activities, such as emergency reliefs, or remote area applications, the system should be operated at islanded mode with the grid-forming capability because there is usually no main grid access in these scenarios. The grid-connected operation is also provided inside the SPEED system for normal daily scenarios, where the energy generated by the PV source can be sent to the main grid.

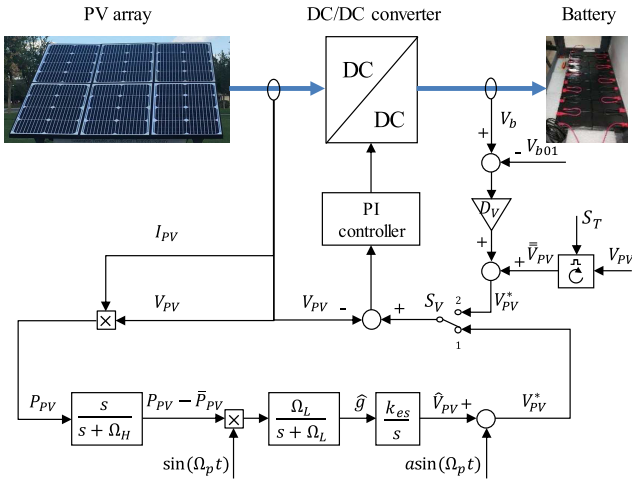

FIGURE 4. DC/DC boost converter control.

III. CONTROL SYSTEM DESIGN

In order to achieve autonomous operation of the SPEED system in a stable, reliable and flexible manner, advanced power electronics control technologies are developed and embedded into both DC-DC boost converter and DC-AC converter control in the SYNDEM power converter. With the implementation of the advanced control algorithms, the MPPT function for PV source, islanded mode operation and grid-connected mode operation of the SPEED system, and the protections for both battery overcharging and battery overdischarging are achieved. The data monitoring subsystem is developed to monitor and record both system operation data and control data through the RS485 communication with the SYNDEM power converter.

A. DC/DC BOOST CONVERTER CONTROL

As shown in Fig. 2(b), the output power of the PV source varies, according to different solar irradiations or load conditions. In order to achieve the maximal power acquisition of the PV source, an ES-based MPPT algorithm [19], [28], [34] is adopted for the DC/DC boost converter control with battery charging. In MPPT mode, the output power of the PV source should be maximized, where a digital switch S_V is switched to position 1 in MPPT mode operation, as illustrated in Fig. 4. A small perturbation, $a\sin(\Omega_p t)$, is added to the reference voltage of PV source V^*_{PV}. Then, through the proportional–integral (PI) controller of the PV source voltage V_{PV}, the power output of PV source P_{PV} will be perturbed accordingly. Through a high pass filter $\frac{s}{s+\Omega_H}$, the DC part of the P_{PV} will be filtered out, and the perturbation signal is left. The multiplication of the perturbation signal $P_{PV}-\overline{P}_{PV}$ by $\sin(\Omega_p t)$ results in an estimation of the gradient of $P_{PV}-V_{PV}$ curve, which is smoothed by a low-pass filter $\frac{\Omega_L}{s+\Omega_L}$. This gradient $\hat{g}$ is used to tune the moving direction of the reference voltage of PV source V^*_{PV}. Through multiple tunings of the reference voltage V^*_{PV} with an integral function $\frac{k_{es}}{s}$, the optimal point of the PV source will be achieved. k_{es} is a positive constant gain to adjust the convergence rate of the ES-based control.

As a P&O optimal algorithm, the ES-based control will always seek the optimal point of the target system. This might cause the overcharging issue of the battery pack during the long-term operation, if the PV power is much larger than the load consumption at islanded mode operation. In order to avoid this issue, a PV voltage droop control algorithm based on the battery voltage is provided, as demonstrated in Fig. 4. When the battery voltage V_b is higher than a voltage-protection trigger point V_{b01}, the digital switch S_V

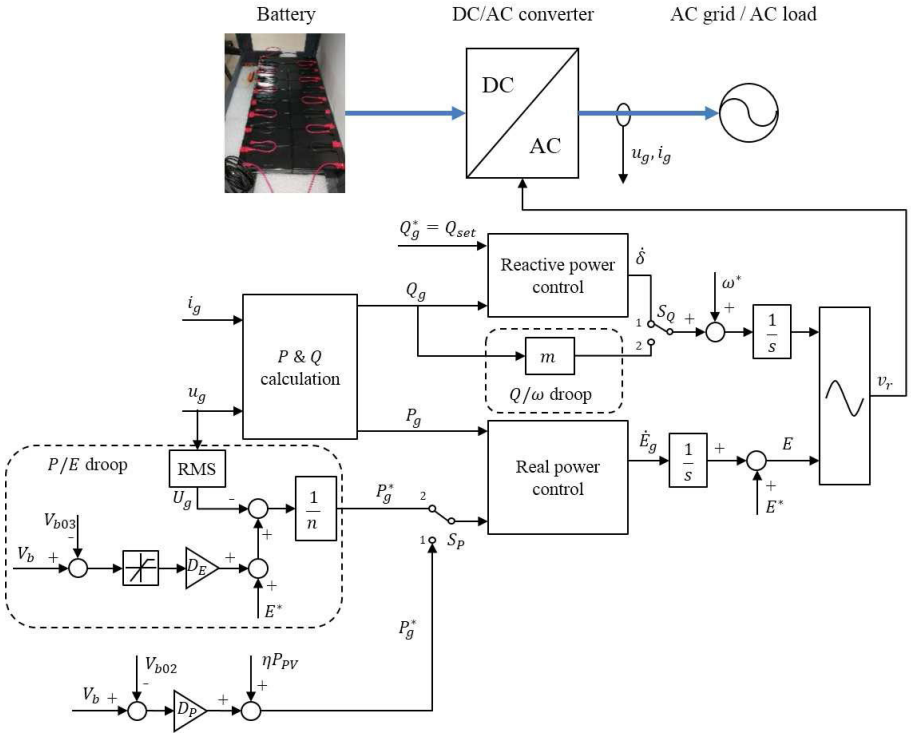

FIGURE 5. DC/AC converter control.

will be changed to position 2, and the memory function of the PV voltage V_{PV} will be triggered and saved by the digital switch S_T, where $\bar{V}_{PV}$ is the saved PV voltage V_{PV}. The reference voltage of the PV source is designed as

$$V_{PV}^* = \bar{V}_{PV} + D_V(V_b - V_{b01}) \tag{1}$$

where D_V is a positive droop coefficient. When the battery voltage V_b increases with the injected PV power, V_{PV}^* will increase as well through this PV voltage droop function (1). This means that the output power of the PV source will decrease along with the increasing of the V_{PV}^* and the PV voltage control, according to Fig. 2(b). The D_V can be selected to fulfill that, when the battery voltage V_b reaches its maximal value, the PV voltage V_{PV} will reach its open-circuit point, then the PV source will not output any power to charge the battery pack. In this way, the overcharging issue of the battery pack can be naturally avoided. It is worth noting that a hysteresis band can be designed for V_{b01} to avoid frequent switching between the ES-based control and the PV voltage droop control at the trigger point V_{b01}.

The PV voltage is regulated by a PI controller

$$u = -k_{ppv}(V_{PV}^* - V_{PV}) - k_{ipv}\int (V_{PV}^* - V_{PV})dt \tag{2}$$

where u is the duty cycle for the DC/DC boost converter, V_{PV}^* is from the MPPT unit or the PV voltage droop control, and $k_{ppv} > 0$ and $k_{ipv} > 0$ are PI gains. Note that the PI controller for the PV voltage regulation has negative gains, according to the right hand side of the power–voltage curve in Fig. 2(b), where the PV source usually operates from open-circuit point to maximum output power point with MPPT algorithm.

B. DC/AC CONVERTER CONTROL

There are two operation modes for the SPEED system: grid-connected mode and islanded mode. Different operation modes are achieved through the DC/AC converter control. In this paper, the voltage source-based robust power flow control [26] and the voltage source-based robust droop control [18] are integrated together to facilitate the operation of the SPEED system under two modes in a unified framework, as shown in Fig. 5. Also, the battery voltage balance control in grid-connected mode and the overdischarging protection of the battery pack in islanded mode are further developed in the DC/AC converter control.

1) GRID-CONNECTED MODE OPERATION OF THE DC/AC CONVERTER

In normal daily scenarios, when the main grid is detected, the DC/AC converter will automatically operate at grid-connected mode, and the electricity generated by the PV source will be sent to the main grid. In order to achieve robust integration of the SPEED system into the main grid, the voltage source-based robust power flow control [26] is embedded into the DC/AC converter control. It can achieve a grid-friendly manner and reject various disturbances, such as the fluctuations of the battery voltage, variations of output

impedance or line impedance, and variations of both grid voltage and grid frequency.

As demonstrated in [26], [29], considering the voltage source $E\angle\delta$, or the output voltage of a DC/AC converter, delivering the power to the main grid $U_g\angle 0^o$ through an impedance $Z_o\angle\theta$, the real power P_g and the reactive power Q_g received by the grid $U_g\angle 0^o$ can be obtained as

$$P_g = \left(\frac{EU_g}{Z_o}\cos\delta - \frac{U_g^2}{Z_o}\right)\cos\theta + \frac{EU_g}{Z_o}\sin\delta\sin\theta \quad (3)$$

$$Q_g = \left(\frac{EU_g}{Z_o}\cos\delta - \frac{U_g^2}{Z_o}\right)\sin\theta - \frac{EU_g}{Z_o}\sin\delta\cos\theta \quad (4)$$

where δ is called power angle. Following the procedures in [26], and taking the time derivative of both (3) and (4), the dynamics of power delivery are expressed in

$$\dot{P}_g = \frac{EU_g\dot{\delta}}{Z_o}\cos\delta\sin\theta - \frac{EU_g\dot{\delta}}{Z_o}\sin\delta\cos\theta + \frac{U_g\dot{E}}{Z_o}\cos\delta\cos\theta + \frac{U_g\dot{E}}{Z_o}\sin\delta\sin\theta \quad (5)$$

$$\dot{Q}_g = \frac{U_g\dot{E}}{Z_o}\cos\delta\sin\theta - \frac{EU_g\dot{\delta}}{Z_o}\sin\delta\sin\theta - \frac{EU_g\dot{\delta}}{Z_o}\cos\delta\cos\theta - \frac{U_g\dot{E}}{Z_o}\sin\delta\cos\theta \quad (6)$$

For this SPEED system, the resistance-type impedance converter or named *R*-converter [29] is considered, therefore, the impedance angle θ and the power angle δ are usually small. Then, the dynamics of power delivery (5) and (6) can be rewritten as

$$\dot{P}_g = \frac{U_g}{Z_o}\dot{E} + \triangle_p \quad (7)$$

$$\dot{Q}_g = -\frac{EU_g}{Z_o}\dot{\delta} + \triangle_q \quad (8)$$

where

$$\triangle_p = \frac{U_g\dot{E}}{Z_o}(\cos\delta\cos\theta - 1) + \frac{EU_g\dot{\delta}}{Z_o}\cos\delta\sin\theta - \frac{EU_g\dot{\delta}}{Z_o}\sin\delta\cos\theta + \frac{U_g\dot{E}}{Z_o}\sin\delta\sin\theta, \quad (9)$$

$$\triangle_q = -\frac{EU_g\dot{\delta}}{Z_o}(\cos\delta\cos\theta - 1) + \frac{U_g\dot{E}}{Z_o}\cos\delta\sin\theta - \frac{U_g\dot{E}}{Z_o}\sin\delta\sin\theta - \frac{U_g\dot{E}}{Z_o}\sin\delta\cos\theta, \quad (10)$$

are the lumped uncertain terms, including the uncertainties, the nonlinearity, and the coupling effects of the power delivery model. As illustrated in Fig. 5, both P_g and Q_g can be calculated by a *P&Q* calculation unit [18], [29].

According to a robust control method, the UDE-based control in [35], and the procedure in [26], the robust power flow control for both real power control and reactive power control can be designed for the power delivery dynamics (7) and (8) as follows

$$\dot{E} = \frac{Z_o}{U_g}\left[L^{-1}\left\{\frac{1}{1-G_{pf}(s)}\right\} * (\dot{P}_g^* + k_p e_p) - L^{-1}\left\{\frac{sG_{pf}(s)}{1-G_{pf}(s)}\right\} * P_g\right], \quad (11)$$

$$\dot{\delta} = -\frac{Z_o}{EU_g}\left[L^{-1}\left\{\frac{1}{1-G_{qf}(s)}\right\} * (\dot{Q}_g^* + k_q e_q) - L^{-1}\left\{\frac{sG_{qf}(s)}{1-G_{qf}(s)}\right\} * Q_g\right]. \quad (12)$$

where P_g^* is a real power reference, and Q_g^* is a reactive power reference. $e_p = P_g^* - P_g$ and $e_q = Q_g^* - Q_g$ are tracking errors. $k_p > 0$ and $k_q > 0$ are error feedback gains in the UDE-based control. $G_{pf}(s)$ and $G_{qf}(s)$ are UDE filters to estimate the unknown terms $\triangle_p$ in (7) and $\triangle_q$ (8). The nominal real power reference can be set as

$$P_g^* = \eta P_{PV} \quad (13)$$

where P_{PV} is the output power of the PV source, η is the approximated system efficiency close to 1. This means that most of power generated by the PV source will be delivered to the main grid. The reactive power reference Q_g^* can be arbitrarily set within the allowed range, and normally Q_g^* is set to zero with $Q_{set} = 0$ to keep unity power factor.

In order to further prevent the overcharging or overdischarging of the battery pack in grid-connected mode, a real power set point droop algorithm based on the battery voltage is added into the real power reference

$$P_g^* = \eta P_{PV} + D_P(V_b - V_{b02}) \quad (14)$$

where D_P is a positive droop coefficient. When the battery voltage V_b is higher (lower) than a voltage-protection trigger point V_{b02}, more (less) power will be delivered to the grid, and the battery voltage V_b will decrease (increase) accordingly to keep both power balance and voltage balance of the battery pack. Through this real power set point droop function (14), the battery voltage can be always regulated within a narrow range around the trigger point V_{b02}, where D_P can be used to tune the voltage range of the battery pack. In this way, both overcharging and overdischarging issues of the battery pack are naturally avoided in grid-connected mode. It is noted that there is no need of a hysteresis band for the trigger point V_{b02}.

As shown in Fig. 5, in grid-connected mode, both the digital switch S_P and the digital switch S_Q are switched to position 1. Furthermore, through the combination $\dot{\delta}$, ω^*, $\dot{E}$, and E^*, a final sinusoidal voltage reference v_r will be generated for the operation of the DC/AC converter, where ω^* and E^* are rated grid frequency and rate grid voltage, respectively.

2) ISLANDED MODE OPERATION OF THE DC/AC CONVERTER

When the SPEED system is deployed for outdoor activities, it needs to be operated at islanded mode. For the islanded mode operation of the DC/AC converter, the control objectives are to provide both voltage regulation and frequency regulation

with the capabilities of grid-forming, and to keep the power balance between power sources and loads. To achieve these functions, the idea of the voltage source-based robust droop control technology [18] is further embedded into the DC/AC converter control to enhance system robustness.

In the islanded mode, both the digital switch S_P and the digital switch S_Q are switched to position 2, as shown in Fig. 5. A Q/ω droop unit with

$$\omega = \omega^* + mQ_g \tag{15}$$

is provided for frequency regulation, where m is a positive droop coefficient for reactive power, which is correlated with the power capacity of the SPEED system. Normally, mQ_g is designed as a very small value to keep the small band of the DC/AC converter output frequency around the rated value ω^*. In other aspect, for the potential parallel operation of multiple SPEED systems, all systems can work under the same frequency ω at steady state [18]. Therefore, all parallel SPEED systems will have same mQ_g, which guarantees the accurate sharing of the reactive power for multiple SPEED systems [29].

As shown in Fig. 5, a P/E droop unit is combined with real power control (12) for voltage regulation. Normally, the real power reference P_g^* is designed as

$$P_g^* = \frac{E^* - U_g}{n} \tag{16}$$

where U_g is the root-mean-square (RMS) value of the instantaneous load voltage u_g, and n is a positive droop coefficient for real power, which is also correlated with the power capacity of the SPEED system. At steady state, the real power output P_g will track the reference P_g^* through the real power control (11)

$$P_g = P_g^* = \frac{E^* - U_g}{n}. \tag{17}$$

Nominally, nP_g is also designed as a small value to keep the small band of the output voltage U_g of the DC/AC converter around the rated value E^*. In other aspect, for the potential parallel scenarios, nP_g is same for all parallel SPEED systems, because both E^* and U_g are same for all parallel-operated units, which guarantees accurate sharing of the real power for multiple SPEED systems.

Additionally, the robust droop control designed in this paper is an improved version of the conventional droop controller [25] by introducing the load-voltage feedback and the UDE-based robust control algorithm. In addition to the voltage/frequency regulation, accurate power sharing and robustness to handle uncertainties and disturbances, the UDE-based robust droop control still inherits the advantages of the conventional droop control, such as, no communication requirement, autonomous power balance between power sources and loads, and the "plug and play" feature.

In order to further prevent the overdischarging of the battery pack in islanded mode operation, especially within a single SPEED system, an AC voltage set point droop control algorithm based on the battery voltage is added into the real power reference

$$P_g^* = \frac{\left[E^* + D_E \cdot \text{sat}(V_b - V_{b03})\right] - U_g}{n} \tag{18}$$

where D_E is a positive droop coefficient, and the saturation function is defined as

$$\text{sat}(V_b - V_{b03}) = \begin{cases} 0, & V_b \geq V_{b03}, \\ V_b - V_{b03}, & V_b < V_{b03}. \end{cases} \tag{19}$$

When the battery voltage V_b is higher than a voltage-protection trigger point V_{b03}, a normal P/E droop function is provided. If the battery voltage V_b is lower than the trigger point V_{b03}, instead of the voltage set point E^*, the voltage set point is changed to $E^* + D_E(V_b - V_{b03})$. Then the output voltage U_g of the DC/AC converter will decrease accordingly, which can reduce the power consumption of the loads. The D_E can be selected to fulfill that, when the battery voltage V_b reaches its minimal value, the output voltage U_g of the DC/AC converter will decrease to zero. Through this AC voltage set point droop function (18), the overdischarging issue of the battery pack is naturally avoided in islanded mode. It is noted that there is no need of a hysteresis band for the trigger point V_{b03}.

TABLE 1. The data frame from the SYNDEM power converter to the data monitoring subsystem through RS485 communication.

Data definition	Data type	Factor	Offset
Header	8-bit	1	0
Counter	16-bit	1	0
PV voltage (V)	16-bit	0.1	0
PV power (W)	16-bit	0.1	0
Battery voltage (V)	16-bit	0.1	0
Real power output (W)	16-bit	0.1	-1000
Reactive power output (Var)	16-bit	0.1	-1000
AC RMS current (A)	16-bit	0.1	0
AC RMS voltage (V)	16-bit	0.1	0
Frequency (Hz)	16-bit	0.1	0
Error code	16-bit	1	0
Check sum	16-bit	1	0
Terminator	8-bit	1	0

C. DATA MONITORING SUBSYSTEM

The data monitoring subsystem is developed to acquire and visualize the real-time data of the SPEED system. In this work, the open source Qt C++ and Node.Js frameworks are used for software development on the Raspberry-Pi single board computer. As shown in the Fig. 6, the architecture of the data monitoring subsystem consists of two applications: the data concentrator and human machine interface (HMI) application, and the web server application.

In the data concentrator and HMI application, the serial interface is used to communicate with the SYNDEM power converter through the RS485 communication; the HMI is used for data visualization on GUI; the asynchronous TCP/IP data server is used for data exchange with the web server application; and the data concentration handles the raw data and manages the data pool. Both data concentration and serial

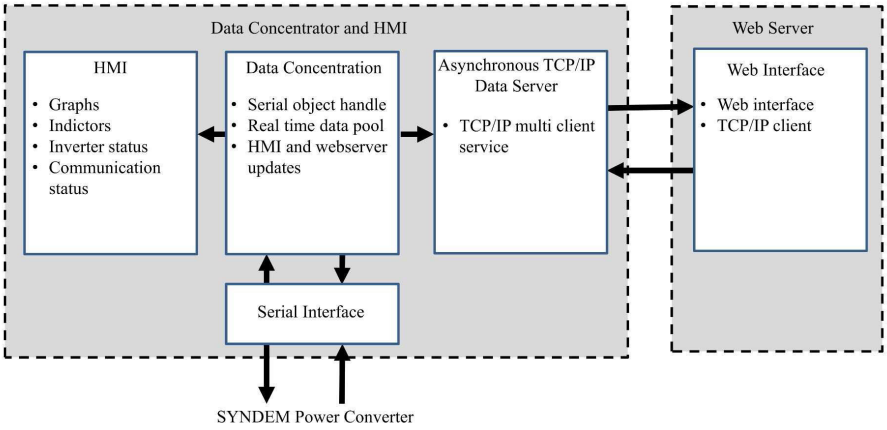

FIGURE 6. Data monitoring subsystem software architecture.

Algorithm 1 Algorithm for Data Reading Through RS485 Serial Communication

Require: ReadTimer (100 ms), SerialPort (9600 bps, 1 stop bit, even parity), *DataFrameLenght* = 13, AccesData
Ensure: *DataPool*

```
if ReadTimer is elapsed and SerialPort is opened then
    Data = Readall (SerialPort)
    Append (Data, AccesData)                          ▷ Append Data to AccesData
    Index = FindStartDelimiterIndex (Data)
    DataPool = Return data containing DataFrameLenght from starting at position index
    AccesData = Return data containing from starting at position index + DataFrameLenght to the end
end if
```

FIGURE 7. The SPEED system: (a) Front view; (b) Back view.

interface are implemented with a 100 ms sampling rate with the fast data acquisition, while the HMI is updated with every 1 s to mitigate the execution overhead of the application. The data frame for RS485 serial communication is illustrated in Table 1. In order to avoid the data loss, Algorithm 1 is used for data acquisition of the serial interface.

The web interface is a Node.js-based application for the remote data monitoring. The user can log into the Wi-Fi access point hosted by the Raspberry Pi and then monitor the real-time data of the SPEED system through a web browsing application (Google chrome, Internet explore, etc.).

IV. FIELD TEST

To enhance the mechanical robustness and portability of the SPEED system, all hardware components, such as, the PV source, the battery pack, the SYNDEM power converter, and the data monitoring subsystem, are mechanically mounted on a moving cart, as shown in Fig. 7 with both front view and back view. The field test of the SPEED system is conducted on TTU campus. A video of the field test can be found in [36]. The parameters of the SYNDEM power converter are referred to [37]. How to choose parameters for the ES-based MPPT can be found in [19], parameters for the robust power flow control in [26], and parameters for the robust droop control in [18]. In three battery protection algorithms, the voltage-protection trigger point V_{b01} is used for overcharging protection, the voltage-protection trigger point V_{b03} for overdischarging protection, and the voltage-protection trigger point V_{b02} for voltage balanced control in grid-connected mode. Therefore, the relationships of V_{b01}, V_{b02}, and V_{b03}

TABLE 2. The key control parameters of the SPEED system.

Parameters	Values	Parameters	Values
Ω_p	10π rad/s	$G_{qf}(s)$	$\frac{20\pi}{s+20\pi}$
a	1.5	Q_g^*	0 Var
k_{es}	4	ω^*	120π rad/s
Ω_H	2π rad/s	E^*	120 V_{rms}
Ω_L	10π rad/s	η	0.96
D_V	2	D_P	50
V_{b01}	260 V	V_{b02}	255 V
k_{ppv}	0.001	m	$2\pi * 10^{-4}$
k_{ipv}	0.01	n	0.01
k_p	10	D_E	4
k_q	2	V_{b03}	230 V
$G_{pf}(s)$	$\frac{20\pi}{s+20\pi}$	-	-

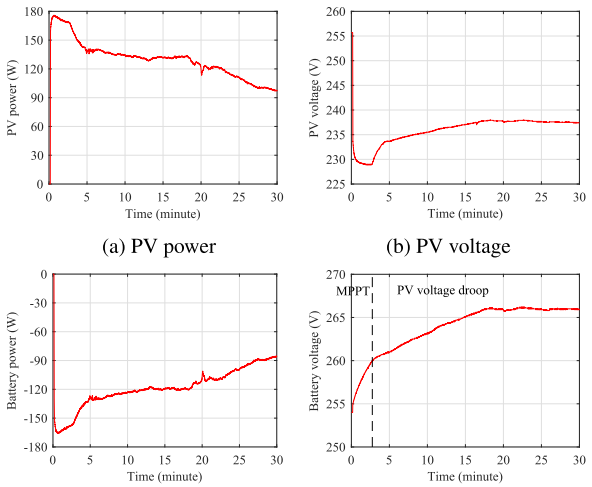

(a) PV power (b) PV voltage

(c) Battery power (d) Battery voltage

FIGURE 8. Case 1: Battery charging with the MPPT (before $t = 2.8$ minute) and the PV voltage droop control (after $t = 2.8$ minute).

should be $V_{b01} > V_{b02} > V_{b03}$. The parameters for battery protection algorithms can be selected based on the characteristics of the lead-acid battery pack and further field-trial tests. The key control parameters are listed in Table 2.

To test different functions and capabilities, e.g., the MPPT, the PV voltage droop control, islanded mode operation, grid-connected mode operation, and the battery protections of the SPEED system, four field test cases are conducted as follows.

A. CASE 1: BATTERY CHARGING WITH MPPT AND PV VOLTAGE DROOP CONTROL

In this scenario, the battery charging with both MPPT and PV voltage droop control is investigated. The system responses are shown in Fig. 8. Before $t = 2.8$ minute, the system operates at the MPPT mode with the ES-based control. The PV power increases to the maximum value, close to 180 W quickly, due to the ES-based MPPT, as shown in Fig. 8(a). Then, the PV power decreases slowly, which is caused by the increase of the temperature of the PV source. The PV voltage decreases along with the power output of the PV source, as shown in Fig. 8(b). It can be noticed that the PV voltage also has slight decrease due to the effects of the temperature. In this case, most of the PV power is injected into the battery pack, because there is no AC power output. The absolute value of the battery power is a little bit lower than the PV power shown in Fig. 8(c), due to the system losses, e.g., power electronics losses, wire losses, and parasitic losses. The negative battery power means that the battery pack is charging. Because the large power is injected into the battery pack, the battery voltage increases quickly, as shown in Fig. 8(d). At $t = 2.8$ minute, the battery voltage reaches the trigger point $V_{b01} = 260$ V, and the system changes to the PV voltage droop mode. In this mode, the PV voltage increases with the battery voltage, as shown in Fig. 8(b) and Fig. 8(d), because the PV voltage set point increases with the battery voltage, according to equation (1). Therefore, the PV power and the absolute value of the battery power decrease accordingly. In this way, the battery pack overcharging issue is naturally avoided. After $t = 20$ minute, the battery pack reaches a dynamic charging balance, and the battery voltage almost keeps a constant value. The PV voltage almost keeps steady as well. Later, the gradual decrease of the PV power is caused by the reduced solar irradiance. Noted that there are no oscillations in both PV power and battery power through the proposed PV voltage droop control, even under varying solar irradiance. With the proposed control, the system can operate at MPPT mode when the battery voltage is lower than the trigger point V_{b01}, and the PV voltage droop control can prevent the battery pack overcharging when the battery voltage is higher than the trigger point V_{b01}.

B. CASE 2: ISLANDED MODE OPERATION

In this scenario, the islanded mode operation of the SPEED system with the grid-forming capability is tested. In order to test the capabilities of the battery pack, the PV source is disabled. Several appliances, e.g., laptops, LEDs, cell phone chargers, drone chargers, and an electric kettle, are used as electrical loads to simulate the emergency or disaster relief scenario. The system responses are shown in Fig. 9. The SPEED system can do a black-start with voltage and frequency regulation. The AC output RMS voltage and AC output frequency for the loads are shown in Fig. 9(b) and Fig. 9(d), respectively. The grid-forming capabilities of this SPEED system are demonstrated at islanded conditions, where the AC output RMS voltage can always be regulated around 120 V_{rms}, and the frequency is always regulated around 60 Hz, during the variations of both load real power in Fig. 9(a) and load reactive power in Fig. 9(c). The load real power is changed with different types of loads. The load reactive power almost keeps constant, because there is a *LC* filter inside the DC/AC converter, and most of loads are resistance-type loads. The battery power is close to the load power as shown in Fig. 9(e). When a large load, e.g., an electric kettle, is added between $t = 19.8$ minute and $t = 30$ minute, the AC voltage has a small decrease because of the P/E droop function (17). The battery voltage almost keeps constant before $t = 19.8$ minute with the small loads, and has a large drop (around 5 V) because of the

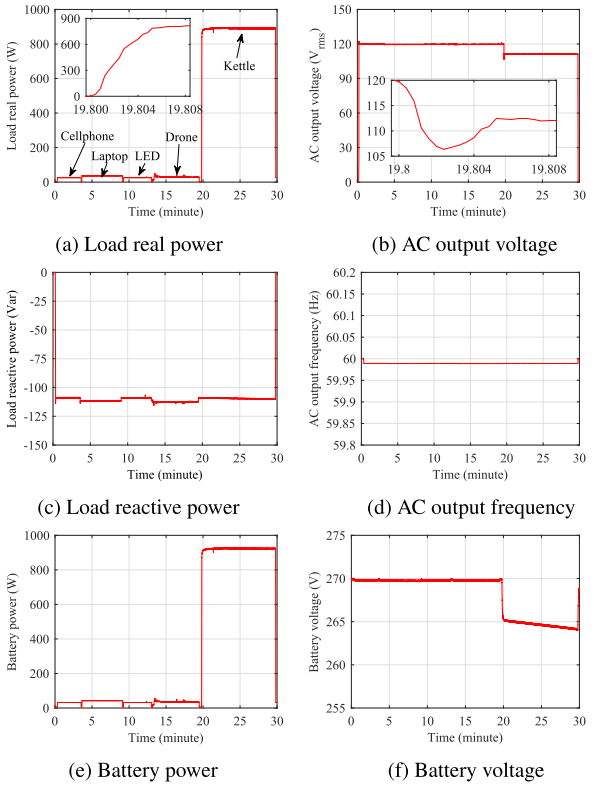

(a) Load real power (b) AC output voltage

(c) Load reactive power (d) AC output frequency

(e) Battery power (f) Battery voltage

FIGURE 9. Case 2: Islanded mode operation to simulate the emergency or disaster relief scenario.

large electric kettle load, as shown in Fig. 9(f). The battery voltage also decreases slowly after $t = 19.8$ minute, which is caused by the power consumption of the loads. The transient responses of both load real power and AC output RMS voltage at $t = 19.8$ minute are enlarged in Fig. 9(a) and Fig. 9(b), respectively. The transient response speed of the load real power is around 0.008 minute, i.e., 480 ms. This slow response is mainly caused by the calculation of the real power through a low-pass filter with the cut-off frequency of 6 Hz. The AC output RMS voltage only drops slightly, and converges to a steady state quickly, within 0.005 minute, i.e., 300 ms. The transient AC output voltage and AC load current under a nonlinear load (with the drone charging) and a linear load (with the electric kettle) are shown in Fig. 10(a) and Fig. 10(b), respectively.

C. CASE 3: BATTERY PROTECTION UNDER A LOW BATTERY VOLTAGE

In this scenario, the battery protection under a low battery voltage with AC voltage set point droop control is studied. Similar to Case 2, the SPEED system is initially operated at the islanded mode with an electric kettle load, where the battery pack is almost run out. The system responses are shown in Fig. 11. Before $t = 12$ minute, the battery voltage is higher than the voltage-protection trigger point V_{b03}, as shown in Fig. 11(a). The system has same AC output voltage shown in Fig. 11(b) and load real power shown in Fig. 11(d) with normal operation, compared to Case 2 shown in Fig. 9(a)

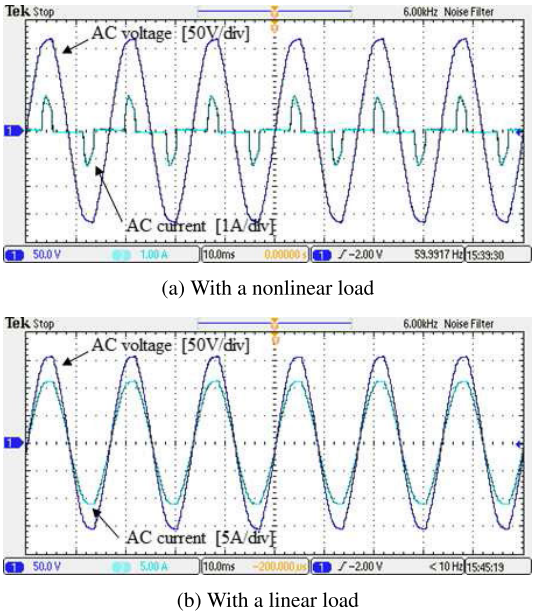

(a) With a nonlinear load

(b) With a linear load

FIGURE 10. Case 2: Transient AC output voltage and AC load current under nonlinear and linear loads.

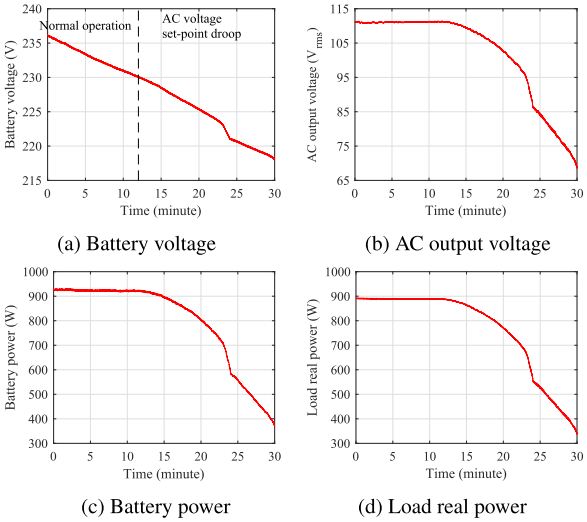

(a) Battery voltage (b) AC output voltage

(c) Battery power (d) Load real power

FIGURE 11. Case 3: AC voltage set point droop control under a low battery voltage.

and Fig. 9(b) within $20 \sim 30$ minute. After $t = 12$ minute, the battery voltage is lower than the voltage-protection trigger point V_{b03}, the system changes to AC voltage set point droop mode. The AC output voltage decreases gradually, according to the decrease of AC voltage set point, which is affected by the decrease of the battery voltage based on the equation (18). The load real power decreases accordingly, as shown in Fig. 11(d). The battery output power is slightly higher that the load real power in Fig. 11(c), because of the system efficiency. Through this AC voltage set point droop control, the overdischarging issue of the battery pack can be avoided in islanded mode.

D. CASE 4: GRID-CONNECTED MODE OPERATION

In this scenario, the grid-connected mode operation of the SPEED system is tested. The system responses are shown

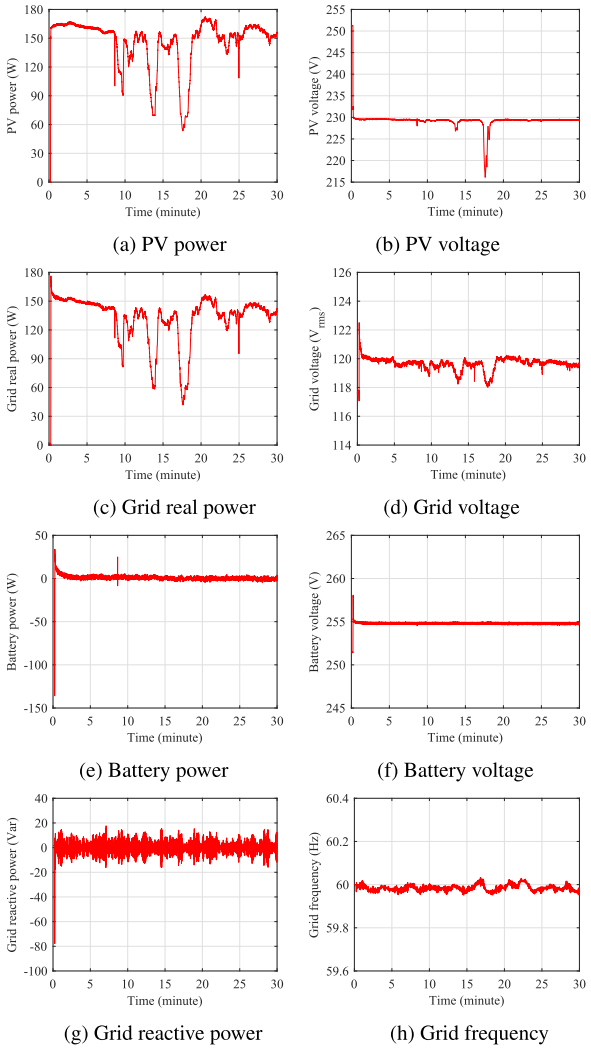

FIGURE 12. Case 4: Grid-connected mode operation.

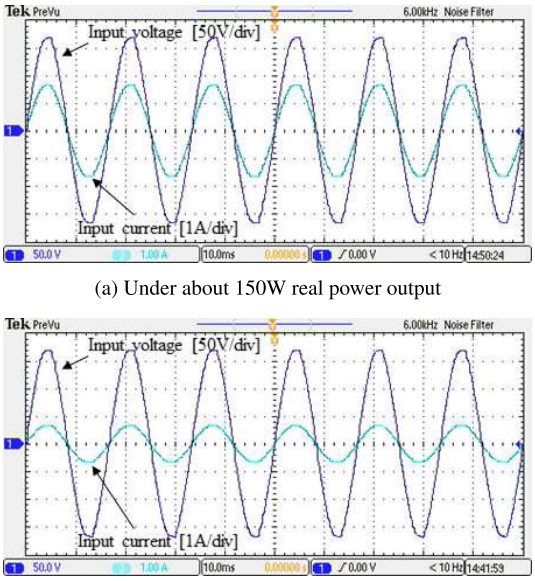

FIGURE 13. Case 4: Transient AC grid voltage and transient AC output current under different power outputs.

in Fig. 12. When the system is connected to the main grid, the grid-connected mode operation of the SPEED system is triggered. The PV system always operates at the MPPT mode. When the system starts, the PV power increases to the maximum value, around 160 W quickly, due to the fast convergence of the ES-based MPPT, as shown in Fig. 12(a). The changes of the PV power are caused by the varying sunlight conditions and the changes of the PV temperature. During $t = 8$ minute to $t = 18$ minute, there are large variances in PV power, due to the PV shading effect from the moving clouds. The PV shading also affects the PV voltage, as shown in Fig. 12(b), and there is a large voltage drop around $t = 17.5$ minute with the fully blocked sunlight. The grid real power follows the trend of PV power well, as shown Fig. 12(c). The grid real power is slightly smaller than the PV power after $t = 2$ minute, because of the system efficiency. With the proposed battery voltage balance control (14), the battery power is almost kept around zero at steady state (after $t = 2$ minute), as shown in Fig. 12(e), and the battery voltage is kept at the trigger point $V_{b02} = 255$ V as shown in Fig. 12(f). Before $t = 2$ minute, the battery power is greater than zero, and the grid real power is greater than the PV power, as the battery voltage is higher than the trigger point V_{b02}. The negative battery power at initial state is because the DC/AC controller is enabled after the DC/DC controller, and there is a short-term battery charging. The grid reactive power is always regulated around 0 Var to keep the unity power factor, as shown in Fig. 12(g). The reasons for small spikes of both grid real power and grid reactive power are from different aspects, e.g., measurement noises, small disturbances for both grid voltage and grid frequency. It can be noticed that both grid voltage and grid frequency are varying, as shown in Fig. 12(d) and Fig. 12(h), because there is a high penetration of renewables in the Texas grid. The proposed control still can regulate the grid real power and the grid reactive power well with the robust performances. Both the waveforms of the transient grid voltage and the transient DC/AC output current under different power outputs are shown in Fig. 13(a) and Fig. 13(b), respectively.

V. CONCLUSION

In this paper, a SPEED system has been proposed for applications associated with disaster relief or remote areas, and a prototype system has been built and tested on TTU campus. Advanced power electronics control technologies have been developed to achieve the MPPT function for the PV source, the islanded mode operation and the grid-connected mode operation, and the battery overcharging and overdischarging protections. Both islanded mode and grid-connected mode operations of the SPEED system are achieved through voltage source-based control techniques within a unified control framework to integrate the robust droop control and the robust power flow control without the requirement of the PLL. This enables the grid-forming capability and the scalability of the

SPEED system. The PV voltage droop control algorithm has been proposed to avoid both the battery pack overcharging and the power oscillation under varying solar irradiation or shading. The autonomous operation of the SPEED system is achieved without the requirement of the extra power management system or energy management system, and the proposed control design and communication design are implemented in a widely-used TI TMS320F28335 MCU to enhance the feasibility of the proposed SPEED system. The field test results have demonstrated the effectiveness of the proposed SPEED system under different operation conditions. In conclusion, the proposed SPEED system has shown great potential in contributing to sustainable and portable electricity demand during emergency/disaster relief and energy harvesting.

REFERENCES

[1] I. J. Balaguer, Q. Lei, S. Yang, U. Supatti, and F. Z. Peng, "Control for grid-connected and intentional islanding operations of distributed power generation," *IEEE Trans. Ind. Electron.*, vol. 58, no. 1, pp. 147–157, Jan. 2011.

[2] J. Green and P. Newman, "Disruptive innovation, stranded assets and forecasting: The rise and rise of renewable energy," *J. Sustain. Finance Investment*, vol. 7, no. 2, pp. 169–187, Apr. 2017.

[3] J. Furman, *Economic Benefits of Increasing Electric Grid Resilience to Weather Outages*. Washington, DC, USA: Council of Economic Advisers, Executive Office of the President, 2013.

[4] *Hurricane Irma Cut Power to Nearly Two-Thirds of Florida's Electricity Customers*. Accessed: Sep. 2017. [Online]. Available: https://www.eia.gov/todayinenergy/detail.php?id=32992

[5] *Hurricane Harvey: Texas Power Outages Affect More Than Quarter-Million*. Accessed: Aug. 2017. [Online]. Available: https://www.cbsnews.com/news/hurricane-harvey-texas-power-outages-affect-more-than-255000/

[6] Y. Yuan, L. Wu, W. Song, and Z. Jiang, "Collaborative control of microgrid for emergency response and disaster relief," in *Proc. Int. Conf. Sustain. Power Gener. Supply*, Apr. 2009, pp. 1–5.

[7] C. Abbey, D. Cornforth, N. Hatziargyriou, K. Hirose, A. Kwasinski, E. Kyriakides, G. Platt, L. Reyes, and S. Suryanarayanan, "Powering through the storm: Microgrids operation for more efficient disaster recovery," *IEEE Power Energy Mag.*, vol. 12, no. 3, pp. 67–76, May 2014.

[8] A. Arab, A. Khodaei, Z. Han, and S. K. Khator, "Proactive recovery of electric power assets for resiliency enhancement," *IEEE Access*, vol. 3, pp. 99–109, 2015.

[9] A. Nasipuri, R. Cox, J. Conrad, L. Van der Zel, B. Rodriguez, and R. McKosky, "Design considerations for a large-scale wireless sensor network for substation monitoring," in *Proc. IEEE Local Comput. Netw. Conf. (LCN)*, Oct. 2010, pp. 866–873.

[10] S. M. S. Hussain, A. Tak, T. S. Ustun, and I. Ali, "Communication modeling of solar home system and smart meter in smart grids," *IEEE Access*, vol. 6, pp. 16985–16996, 2018.

[11] P. C. Ghosh, B. Emonts, and D. Stolten, "Comparison of hydrogen storage with diesel-generator system in a PV–WEC hybrid system," *Sol. Energy*, vol. 75, no. 3, pp. 187–198, Sep. 2003.

[12] D. Butler, "Requirements for batteries in remote-area power-supply systems based on technical modelling and field experience," *J. Power Sour.*, vol. 59, nos. 1–2, pp. 99–105, Mar. 1996.

[13] S. Qazi, *Standalone Photovoltaic (PV) Systems for Disaster Relief and Remote Areas*. Amsterdam, The Netherlands: Elsevier, 2016.

[14] *ANSI C84.1-2016: American National Standard for Electric Power Systems and Equipment-Voltage Ratings (60 Hertz)*. ANSI, New York, NY, USA, 2016.

[15] Q.-C. Zhong, "Virtual synchronous machines: A unified interface for grid integration," *IEEE Power Electron. Mag.*, vol. 3, no. 4, pp. 18–27, Dec. 2016.

[16] Z. Yi, W. Dong, and A. H. Etemadi, "A unified control and power management scheme for PV-battery-based hybrid microgrids for both grid-connected and islanded modes," *IEEE Trans. Smart Grid*, vol. 9, no. 6, pp. 5975–5985, Nov. 2018.

[17] Q.-C. Zhong, "Robust droop controller for accurate proportional load sharing among inverters operated in parallel," *IEEE Trans. Ind. Electron.*, vol. 60, no. 4, pp. 1281–1290, Apr. 2013.

[18] Q.-C. Zhong, Y. Wang, and B. Ren, "UDE-based robust droop control of inverters in parallel operation," *IEEE Trans. Ind. Electron.*, vol. 64, no. 9, pp. 7552–7562, Sep. 2017.

[19] Y. Wang and B. Ren, "Fault ride-through enhancement for grid-tied PV systems with robust control," *IEEE Trans. Ind. Electron.*, vol. 65, no. 3, pp. 2302–2312, Mar. 2018.

[20] A. Choudar, D. Boukhetala, S. Barkat, and J.-M. Brucker, "A local energy management of a hybrid PV-storage based distributed generation for microgrids," *Energy Convers. Manage.*, vol. 90, pp. 21–33, Jan. 2015.

[21] A. Merabet, K. Tawfique Ahmed, H. Ibrahim, R. Beguenane, and A. M. Y. M. Ghias, "Energy management and control system for laboratory scale microgrid based Wind-PV-Battery," *IEEE Trans. Sustain. Energy*, vol. 8, no. 1, pp. 145–154, Jan. 2017.

[22] H. Zhu, D. Zhang, B. Zhang, and Z. Zhou, "A nonisolated three-port DC–DC converter and three-domain control method for PV-battery power systems," *IEEE Trans. Ind. Electron.*, vol. 62, no. 8, pp. 4937–4947, Aug. 2015.

[23] J. Hong, J. Yin, Y. Liu, J. Peng, and H. Jiang, "Energy management and control strategy of photovoltaic/battery hybrid distributed power generation systems with an integrated three-port power converter," *IEEE Access*, vol. 7, pp. 82838–82847, 2019.

[24] H. Mahmood, D. Michaelson, and J. Jiang, "Decentralized power management of a PV/battery hybrid unit in a droop-controlled islanded microgrid," *IEEE Trans. Power Electron.*, vol. 30, no. 12, pp. 7215–7229, Dec. 2015.

[25] M. C. Chandorkar, D. M. Divan, and R. Adapa, "Control of parallel connected inverters in standalone AC supply systems," *IEEE Trans. Ind. Appl.*, vol. 29, no. 1, pp. 136–143, Jan./Feb. 1993.

[26] Y. Wang, B. Ren, and Q.-C. Zhong, "Robust power flow control of grid-connected inverters," *IEEE Trans. Ind. Electron.*, vol. 63, no. 11, pp. 6887–6897, Nov. 2016.

[27] R. Leyva, C. Alonso, I. Queinnec, A. Cid-Pastor, D. Lagrange, and L. Martinez-Salamero, "MPPT of photovoltaic systems using extremum–seeking control," *IEEE Trans. Aerosp. Electron. Syst.*, vol. 42, no. 1, pp. 249–258, Jan. 2006.

[28] A. Ghaffari, M. Krstic, and S. Seshagiri, "Power optimization for photovoltaic microconverters using multivariable Newton-based extremum seeking," *IEEE Trans. Control Syst. Technol.*, vol. 22, no. 6, pp. 2141–2149, Nov. 2014.

[29] Q.-C. Zhong and T. Hornik, *Control of Power Inverters in Renewable Energy and Smart Grid Integration*. Hoboken, NJ, USA: Wiley, 2013.

[30] *SYNDEM Smart Grid Research and Educational Kit*. [Online]. Available: https://www.mathworks.com/products/connections/product_detail/syndem-smart-grid-kit.html

[31] S. Liyanage, Y. Wang, Y. Dong, and B. Ren, "A sustainable, portable, and efficient electricity delivery (SPEED) system," in *Proc. IEEE Green Technol. Conference(GreenTech)*, Apr. 2019, pp. 1–4.

[32] D. L. Evans, W. A. Facinelli, and L. P. Koehler, *Simulation and Simplified Design Studies of Photovoltaic Systems*. Springfield, VA, USA: Sandia National Laboratories, 1980.

[33] G. Vachtsevanos and K. Kalaitzakis, "A hybrid photovoltaic simulator for utility interactive studies," *IEEE Trans. Energy Convers.*, vol. EC-2, no. 2, pp. 227–231, Jun. 1987.

[34] K. B. Ariyur and M. Krstic, *Real-Time Optimization by Extremum-Seeking Control*. Hoboken, NJ, USA: Wiley, 2003.

[35] Q.-C. Zhong and D. Rees, "Control of uncertain LTI systems based on an uncertainty and disturbance estimator," *J. Dyn. Syst., Meas., Control*, vol. 126, no. 4, pp. 905–910, Dec. 2004.

[36] *Sustainable, Portable, and Efficient Electricity Delivery (SPEED)_ Prototype V2.0*. Accessed: Jan. 2019. [Online]. Available: https://www.youtube.com/watch?time_continue=10&v=uVcM5kwRhQ0

[37] *SYNDEM Smart Grid Research and Educational Kit User Manual*. Accessed: Feb. 2020. [Online]. Available: http://www.syndem.com/SYNDEM_EduKit_Manual.pdf

SANKA LIYANAGE (Member, IEEE) received the B.Sc. Eng. degree in mechanical and manufacturing engineering from the Faculty of Engineering, University of Ruhuna, Srilanka, in 2010. He is currently pursuing the Ph.D. degree with the Department of Mechanical Engineering, Texas Tech University, Lubbock, TX, USA.

His research interests include microgrids, renewable energy, nonlinear control, and SCADA systems.

YEQIN WANG (Member, IEEE) received the B.Eng. degree in automotive engineering from the College of Engineering, China Agricultural University, China, in 2009, the M.Eng. degree in automotive engineering from the Clean Energy Automotive Engineering Center, Tongji University, China, in 2012, and the Ph.D. degree in wind science and engineering from the National Wind Institute, Texas Tech University, USA, in 2019.

He is currently the Director of Technology with the SYNDEM LLC, Willowbrook, IL, USA. His current research interests include power electronics control, renewable energy, and microgrids.

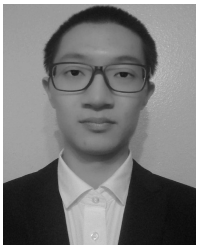

YITING DONG (Graduate Student Member, IEEE) received the B.Eng. degree from the School of Automation Engineering, University of Electronic Science and Technology of China (UESTC), Chengdu, China, in 2014 and the M.Eng. degree in control science and engineering from UESTC, in 2017. He is currently pursuing the Ph.D. degree with the Department of Mechanical Engineering, Texas Tech University, Lubbock, TX, USA.

His current research interests include power electronics control, robust control, and robotics.

BEIBEI REN (Senior Member, IEEE) received the B.Eng. degree in mechanical and electronic engineering and the M.Eng. degree in automation from Xidian University, Xi'an, China, in 2001 and 2004, respectively, and the Ph.D. degree in electrical and computer engineering from the National University of Singapore, Singapore, in 2010.

From 2010 to 2013, she was a Postdoctoral Scholar with the Department of Mechanical and Aerospace Engineering, University of California, San Diego, CA, USA. She is currently an Associate Professor with the Department of Mechanical Engineering, Texas Tech University, Lubbock, TX, USA. Her research focuses on robust control, power electronics control, microgrids and smart grid. She had successful experiences in building microgrid testbeds at different scales for both research and education. She received the TechConnect National Innovation Award for her microgrid control technology. She serves as an Associate Editor for the IEEE TRANSACTIONS ON INDUSTRIAL ELECTRONICS and IEEE ACCESS.